

Assembly of vorticity-aligned hard-sphere colloidal strings in a simple shear flow

Xiang Cheng^{a,1}, Xinliang Xu^{b,1}, Stuart A. Rice^b, Aaron R. Dinner^b, and Itai Cohen^a

^aLaboratory of Atomic and Solid State Physics and Department of Physics, Cornell University, Ithaca, NY 14853; and ^bThe James Franck Institute and Department of Chemistry, The University of Chicago, Chicago, IL 60637

Contributed by Stuart A. Rice, November 7, 2011 (sent for review September 6, 2011)

Colloidal suspensions self-assemble into equilibrium structures ranging from face- and body-centered cubic crystals to binary ionic crystals, and even kagome lattices. When driven out of equilibrium by hydrodynamic interactions, even more diverse structures can be accessed. However, mechanisms underlying out-of-equilibrium assembly are much less understood, though such processes are clearly relevant in many natural and industrial systems. Even in the simple case of hard-sphere colloidal particles under shear, there are conflicting predictions about whether particles link up into string-like structures along the shear flow direction. Here, using confocal microscopy, we measure the shear-induced suspension structure. Surprisingly, rather than flow-aligned strings, we observe log-rolling strings of particles normal to the plane of shear. By employing Stokesian dynamics simulations, we address the mechanism leading to this out-of-equilibrium structure and show that it emerges from a delicate balance between hydrodynamic and interparticle interactions. These results demonstrate a method for assembling large-scale particle structures using shear flows.

colloids | shear-induced structure

The study of ordered structures and symmetries of equilibrium phases in condensed matter is central to our understanding of its various material properties (1). Once driven out of equilibrium, a material can exhibit richer phases with many unexpected structures (2–6). However, the dynamics of these nonequilibrium phases are much less understood relative to their equilibrium counterparts (7–9). Sheared hard-sphere colloidal suspensions provide a simple system for probing many out-of-equilibrium structures. For example, sliding layers in sheared colloidal crystals (10, 11), shear-induced crystallization of colloidal fluids (5), and formation of shear transformation zones—localized regimes of shear-induced structural rearrangement—in colloidal glasses (12) have been observed in such systems.

The simplest and lowest ordered structure predicted to arise from sheared hard-sphere colloidal suspensions is a one-dimensional (1D) string structure, where particles link into strings under shear. This structure has received much attention since it was first found in a numerical simulation (13). Despite intensive study (13–23), however, there is still heated debate over whether such a structure exists in experiments (10, 23, 24) or is an artifact of certain numerical algorithms (20–23). In part, this controversy persists due to the lack of experimental techniques that provide direct visualization of the suspension structure. Since the string structure is predicted to exist in less concentrated suspensions below the crystallization threshold, previous scattering experiments, which average over large sample volumes, have not provided detailed information to unambiguously confirm or disprove the existence of this less regular structure (10, 24). Here, by employing fast confocal microscopy, we show that sheared hard-sphere colloidal suspensions form strings aligned normal to the plane of shear. In combination with Stokesian dynamics simulations (25), we elucidate the mechanical mechanism leading to the observed structures.

Results and Discussion

Experimental Observations of Vorticity-Aligned Strings. Our colloidal suspension consists of $d = 0.96 \mu\text{m}$ silica particles suspended in an index-matched glycerol/water mixture (see *Materials and Methods*). We apply a plane sinusoidal shear to the suspensions with a fixed shear strain amplitude $\gamma = 3.51 \pm 0.16$ and controllable shear angular frequency ω . The structure of particles in the flow (x)—vorticity (z) plane is imaged at different locations along the shear gradient direction (y). With the hard-sphere particles under shear, the relevant dimensionless parameters are the volume fraction of the suspension, ϕ , and the Péclet number $\text{Pe} \equiv \eta_0 \dot{\gamma} d^3 / (8 k_B T)$, which is the ratio of the diffusion and advection time scales. η_0 is the viscosity of the solvent and $\dot{\gamma} = \omega \gamma$ is the amplitude of shear rate.

We explore particle configurations at different Pe in a sample with $\phi = 0.34$, well below the crystallization threshold for hard-sphere colloidal suspensions. The sample is confined between the two shear plates at a separation $h = 7.0d$. At this gap size, the particles form weak layers parallel to the flat shear plates (x - z layers) in equilibrium. These layers enhance strongly with increasing shear (6). We image the particle structure in these x - z layers. Without shear or at low Pe, the particle distribution is nearly isotropic (Fig. 1A). The corresponding pair correlation function, $g(x, z)$, shows a uniform ring for the first shell of neighboring particles (Fig. 1A, *Inset*). However, at intermediate Pe, the suspension develops a string structure, where chains of particles align predominately along the vorticity direction (Fig. 1B). The lifetime of these strings is longer than a full period of the shear cycle and is much longer than our imaging speed (*Movie S1*). This trend is also shown in the change of $g(x, z)$: the ring at low Pe breaks into two crescents along the z direction indicating the 1D symmetry of the string structure (Fig. 1B, *Inset*). As Pe is increased further, the vorticity-aligned string structure becomes more pronounced (Fig. 1C). Although the existence of a string structure is consistent with some simulations (13–19), the orientation of the strings is unexpected: it is normal to the numerically predicted flow direction. To make sure that the vorticity-aligned string structure is not an artifact of our confocal imaging techniques, we perform two numerical and experimental control tests. First, we deshear the raw images by shifting each scan line backwards affinely using the average shear velocity, which cancels any possible shear-induced particle distortions. Second, we switch the shear direction by 90° such that the vorticity direction is normal to the confocal scanning direction. In both controls, we find the same vorticity-aligned string structure at large Pe (Fig. S3).

When samples with higher ϕ are sheared, we find that the vorticity-aligned strings in the x - z layers are pushed closer along the

Author contributions: I.C. designed research; X.C. and X.X. performed research; S.A.R. and A.R.D. designed computational procedure; and X.C., X.X., S.A.R., A.R.D., and I.C. wrote the paper.

The authors declare no conflict of interest.

¹To whom correspondence should be addressed. E-mail: xc92@cornell.edu or xinliang@uchicago.edu.

This article contains supporting information online at www.pnas.org/lookup/suppl/doi:10.1073/pnas.1118197108/-DCSupplemental.

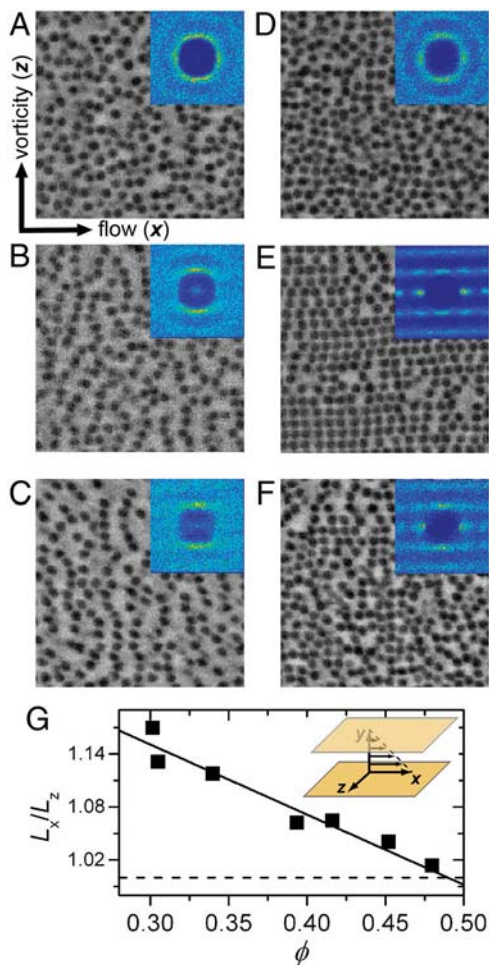


Fig. 1. String structure in sheared colloidal suspensions. (A)–(C) The real-space structures of particles in an x - z layer are shown for a suspension of $\phi = 0.34$ under confinement $h = 7.0d$ at $Pe = 0.72$ (A), $Pe = 72$ (B), and $Pe = 337$ (C). The corresponding pair correlation function $g(x, z)$ is shown in the inset of each plot. $g(x, z)$ is defined as the probability of finding a particle at position (x, z) with respect to the center of each particle. Each $g(x, z)$ measurement averages over about 5,000 particles. The intensity scale in each inset was adjusted for clarity. (D)–(F) show the structure and $g(x, z)$ for the $\phi = 0.46$ sample under otherwise the same experimental conditions as (A)–(C). (G) shows the ratio of the distances between neighboring particles along the x and z directions, L_x/L_z , versus ϕ at $Pe = 70$. $L_x/L_z = 1$ is indicated by the dashed line. The solid line is a linear fit of the data. The inset of (G) shows a definition of our coordinate system. All these measurements are for the 2nd particle layer in the x - z plane counted from the top stationary plate.

direction. Finally, at $\phi = 0.46$ near the crystallization threshold, we observe that strings locally collapse into crystalline islands with fourfold symmetry (Fig. 1 D, E). These square crystalline islands melt gradually at an even higher Pe above 40 (Fig. 1F). To quantify the smooth transition between the string structure and the shear-induced crystalline phase at intermediate Pe , we measure the average distance between neighboring particles along the x and z direction, L_x , L_z , over a range of ϕ (Fig. 1G). L_x/L_z starts at 1.15 for the string structure at low ϕ and approaches 1.0 for the square crystalline phase at high ϕ . L_x/L_z extrapolates to 1.0 at $\phi = 0.50 \pm 0.03$, corresponding to the fluid-crystal transition for hard-sphere suspensions in 3D.

While L_x/L_z and $g(x, z)$ provide detailed information about the distribution of neighboring particle pairs, quantifying larger scale structures requires further analysis. To determine how the resulting string structure depends on the experimental parameters, we perform a cluster analysis. First we identify all the strings within the x - z layers that are aligned along an angle θ with respect to the

flow direction x (Fig. 2 A, B). Then we count the fraction of particles in the strings, $f(\theta)$. Consistent with the direct observations shown in Fig. 1 A–C, we find that with increasing Pe , the flat distribution for $f(\theta)$ develops a strong peak at $\theta = \pi/2$ (Fig. 2C), which indicates the formation of vorticity-aligned strings. In accord with the trends shown in Fig. 1G, with increasing ϕ strings get sufficiently close that our algorithm identifies a significant number of particle strings along the flow direction (Fig. 2D). Furthermore, inside each sample, particles in the x - z layers nearer to the boundary plates—where layering order is strongest (6, 26)—show an enhanced string structure as indicated by the higher peak at $\pi/2$ (Fig. 2E). Consistent with this layering order dependence, we find that decreasing h , which enhances the confinement of samples and hence induces stronger layering order (26), also results in enhanced strings at $\pi/2$ (Fig. 2F).

Measurement of Anisotropic Particle Diffusion. To gain further insight into the symmetry-breaking mechanisms that lead to string formation, we experimentally investigate the microscopic dynamics of individual particles. Specifically, we measure the effective particle diffusion in the x - z plane in the reference frame of the oscillating shear (Fig. 3A). By comparing the effective diffusion constant in the x and z directions, D_x/D_z , we find a broken symmetry in the particle dynamics: with increasing Pe the enhancement of particle diffusion along x is much stronger than enhancement along z (Fig. 3B). Since the experiments are conducted at constant γ , the increase of D_x/D_z cannot be due to Taylor dispersion (27). Owing to the anisotropic particle diffusion, particle density along z has to increase relative to that along x in order to maintain a uniform osmotic pressure within the layer. Consequently, close-packed strings along the vorticity direction gradually emerge with increasing Pe .

Using Stokesian Dynamics Simulations to Determine the Mechanism for String Formation. To parse the contributions from different physical factors to the observed structure and dynamics, we employ Stokesian dynamics simulations (25). In our simulations, spheres immersed in a 3D fluid are confined by an external potential (See *Materials and Methods*). For computational efficiency, we study a small system with only two layers of particles (Fig. 4A) confined by an external potential. We quantify particle structure in the x - z layers with $g(r = d, \theta)$, which corresponds to the first peak of $g(x, z)$ in the polar coordinate (Fig. 4B). In the absence of shear, the suspension equilibrates and $g(r = d, \theta)$ is flat. Under steady shear, our simulation shows a clear signature of vorticity-aligned string structure as indicated by the large peak in $g(r = d, \theta)$ near $\theta = \pi/2$ (Fig. 4B). Thus, our simulation on a small system is already able to capture the basic string formation observed in the experiments.

Two more sets of simulations are performed to test the importance of the hydrodynamic interactions. We first turn off the hydrodynamic interactions between particles. In this limit, the simulations become similar to previous Brownian dynamics simulations of sheared particles (14–17, 19). We find that instead of vorticity-aligned strings, particles form strings aligned along the flow direction, as indicated by the stronger peaks of $g(r = d, \theta)$ near $\theta = 0$ and $\theta = \pi$ in Fig. 4B. This finding highlights the fact that hydrodynamic couplings between particles are essential for formation of vorticity-aligned strings. In another simulation, we turn off the coupling between the rotational motions of particles about their centers and their translational motions. Such a situation would be realized by nonrotating spheres immersed in a liquid with slip boundary conditions. We find that the results are qualitatively similar to the results with full hydrodynamic couplings (Fig. 4B). This finding indicates that the direct coupling between rotational and translational degrees of freedom of particles is not essential for formation of the vorticity-aligned string structure.

